



## Infrared, Raman, and cathodoluminescence studies of impact glasses

Arnold GUCSIK,<sup>1</sup> Christian KOEBERL,<sup>1\*</sup> Franz BRANDSTÄTTER,<sup>2</sup>  
Eugen LIBOWITZKY,<sup>3</sup> and Ming ZHANG<sup>4</sup>

<sup>1</sup>Department of Geological Sciences, University of Vienna, Althanstrasse 14, A-1090 Vienna, Austria

<sup>2</sup>Department of Mineralogy, Natural History Museum, P.O. Box 417, A-1014 Vienna, Austria

<sup>3</sup>Institute of Mineralogy and Crystallography, University of Vienna, Althanstrasse 14, A-1090 Vienna, Austria

<sup>4</sup>Department of Earth Sciences, University of Cambridge, Downing Street, Cambridge, CB2 3EQ, UK

\*Corresponding author. E-mail: [christian.koerberl@univie.ac.at](mailto:christian.koerberl@univie.ac.at)

(Received 4 March 2003; revision accepted 23 April 2004)

**Abstract**—We studied the infrared reflectance (IR), Raman, and cathodoluminescence (CL) spectroscopic signatures and scanning electron microscope-cathodoluminescence (SEM-CL) images of three different types of impact glasses: Aouelloul impact glass, a Muong Nong-type tektite, and Libyan desert glass.

Both backscattered electron (BSE) and CL images of the Muong Nong-type tektite are featureless; the BSE image of the Libyan desert glass shows only weak brightness contrasts. For the Aouelloul glass, both BSE and CL images show distinct brightness contrast, and the CL images for the Libyan desert glass show spectacular flow textures that are not visible in any other microscopic method. Compositional data show that the SiO<sub>2</sub> composition is relatively higher and the Al<sub>2</sub>O<sub>3</sub> content is lower in the CL-bright areas than in the CL-dark regions. The different appearance of the three glass types in the CL images indicates different peak temperatures during glass formation: the tektite was subjected to the highest temperature, and the Aouelloul impact glass experienced a relatively low formation temperature, while the Libyan desert glass preserves a flow texture that is only visible in the CL images, indicating a medium temperature.

All IR reflectance spectra show a major band at around 1040 to 1110 cm<sup>-1</sup> (antisymmetric stretching of SiO<sub>4</sub> tetrahedra), with minor peaks between 745 and 769 cm<sup>-1</sup> (Si-O-Si angle deformation). Broad bands at 491 and 821 cm<sup>-1</sup> in the Raman spectra in all samples are most likely related to diaplectic glass remnants, indicating early shock amorphization followed by thermal amorphization. The combination of these spectroscopic methods allows us to deduce information about the peak formation temperature of the glass, and the CL images, in particular, show glass flow textures that are not preserved in other more conventional petrographic images.

### INTRODUCTION

Impact glasses are found at a variety of impact craters and other locations (e.g., strewn fields) in different regions of the Earth. These glasses are commonly small (generally cm-sized) irregular bodies that occur either directly at an impact crater or are scattered over large areas. Their textures vary from dense to vesicular and slaggy, some contain mineral and rock inclusions, and colors range from blackish to pale green (e.g., McPherson et al. 1984; Koerberl 1986; French 1998).

Commonly, impact glass and tektite characterization has focused on chemical and petrographic studies with only limited spectroscopic investigations (mainly infrared spectroscopy; see Koerberl [1986] and Beran and Koerberl

[1997] for references). High pressure infrared spectra of  $\alpha$ -quartz, coesite, stishovite, and silica glass were obtained by, e.g., Mashimo et al. (1980) and Williams et al. (1993). These authors concluded that the primary effect of compression on the initially tetrahedrally bonded phases is the increased bending of the Si-O-Si bond angle at pressures of less than 10–20 GPa. More recently, Faulques et al. (2001) investigated natural-silica-rich glasses (impactites, tektites, and obsidians) with infrared (IR), Raman, and optical spectroscopy.

Raman and IR active vibrations can be expected if polarizability and dipole moment, respectively, in a molecule change during normal vibrations (Roberts and Beattie 1995); these methods are useful to study the short-range order present in glasses. Cathodoluminescence (CL) is an optical

phenomenon that is based on the generation of visible radiation through sample excitation by high-energetic electrons (in general, energy of incident beam: 5–25 kV; depth of penetration of a sample: 1–3  $\mu\text{m}$ ). Wavelengths of the cathodoluminescence emissions range from the ultraviolet (UV) to the infrared (IR) and result from a variety of defects (e.g., various structural imperfections, such as poor ordering, radiation damage, shock damage) and impurities in the crystal structure of a mineral (Marshall 1988; Hayward 1998).

Here, we present the results of a first combined study of scanning electron microscope-cathodoluminescence (SEM-CL) images and infrared (IR), cathodoluminescence (CL), and Raman spectroscopy of impact glasses. In addition, energy-dispersive X-ray (EDX) compositional data were obtained to determine possible differences between the CL-bright and CL-dark areas. The aim of the study was to determine: a) whether or not different impact glasses show any structure in CL images; b) if there is a systematic difference in CL and Raman properties between impact glasses of different sources; and c) if any structural/compositional information can be gained from these spectroscopic studies.

### SAMPLES

For the present study, we selected three different impact-derived glasses that are characteristic of the range of sample types among such glasses: Aouelloul impact glass (a glass found directly at an impact crater), a Muong Nong-type indochinite tektite (distal impact glass with some known compositional heterogeneity), and Libyan desert glass (a glass of impact origin but without obvious crater association). These glasses were chosen because they represent a range in formation conditions (peak temperature/magnitude of impact event). In the following paragraphs, we provide brief background information on each of these sample types.

The Aouelloul crater is situated at  $20^{\circ}15'N$  and  $12^{\circ}41'W$  in the Adrar region, Western Sahara Desert, Mauritania (e.g., Koeberl 1994). The fission track and K-Ar dating of the impact glass show that this crater was formed  $3.1 \pm 0.3$  Ma ago (Fudali and Cressy 1976; Storzer and Wagner 1977). The 390-m-diameter crater is exposed in an area of Ordovician Oujf quartzite and Zli sandstone (Koeberl et al. 1998). Aouelloul impact glasses contain lechatelierite and baddeleyite (El Goresy 1965; El Goresy et al. 1968), partly digested quartz and feldspar grains, low water content (Beran and Koeberl 1997), and abundant schlieren of different chemical composition (Koeberl 1994). The composition of the glass is similar to that of the sandstone in which the crater is exposed, but some siderophile elements are enriched in the glass (Koeberl and Auer 1991). Re-Os isotope studies of the target sandstone and the impact glass demonstrated the presence of a distinct extraterrestrial component in the glass (Koeberl et al. 1998).

Muong Nong-type tektites are a subgroup of tektites that are abundant in the Australasian strewn field. These tektites differ in some characteristics from “normal” tektites: 1) they have higher concentrations of volatile elements (e.g., Cl, Br, Zn, Cu, Pb); 2) they are chemically inhomogeneous on a mm scale; 3) they contain dark and light layers with different chemical composition; 4) they may contain relict mineral inclusions (e.g., zircon, chromite, rutile, quartz, monazite) (e.g., Glass 1972; Deloule et al. 2001); 5) they contain large and more abundant bubbles that may be ellipsoidal in shape, showing glass flow; 6) they have a large and irregular sample size with no sign of ablation (cf., Koeberl 1992).

Libyan desert glass (LDG) is a natural glass found in an area of about 3500 km<sup>2</sup> between linear sand dunes of the southwestern corner of the Great Sand Sea in western Egypt, near the Libyan border. In terms of chemical composition, LDG is very silica-rich (approximately 98 wt% of SiO<sub>2</sub> content) and has low abundances of most major oxides. The age of LDG was determined by fission-track analysis giving ages ranging from  $28.5 \pm 2.3$  Ma to  $29.4 \pm 0.5$  Ma (plateau age) (e.g., Bigazzi and de Michele 1996; Horn et al. 1997). The origin of LDG has been the subject of much debate since it was discovered early in the 20th century. Evidence for an impact origin includes the presence of lechatelierite (Diemer 1997), baddeleyite (Storzer and Koeberl 1991; Rocchia et al. 1997), and the likely existence of an extraterrestrial component in the glass (e.g., Rocchia et al. 1997; Murali et al. 1997). Previous cathodoluminescence data by Piacenza (1997) were interpreted to show evidence for a granular structure and the presence of lechatelierite. Cathodoluminescence microphotographs were used by Cipriani et al. (2000) in the determination of a possible extraterrestrial body signature in LDG. They concluded that the luminescence of Libyan desert glass is intrinsic not induced by particle damage, as in the case of amorphous silica.

### EXPERIMENTAL PROCEDURES

Polished sections were produced for each sample. IR reflectance spectra were recorded under a vacuum using a Bruker IFS 113v spectrometer. Details of this instrument and analytical conditions are reported by Zhang and Salje (2001) and Zhang et al. (2002). A liquid-nitrogen-cooled MCT detector, a KBr beamsplitter, and a Globar light source were used to record the spectra between 500 and 2500 cm<sup>-1</sup>. Using a commercial reflection accessory from Bruker, we were able to perform close to normal incidence measurements. A spectral resolution of 4 cm<sup>-1</sup> was used for reflectance measurements, as a better resolution did not resolve more spectral features. Gold mirrors were used as references for reflection spectra, and 512 scans were averaged for each spectrum. A homogeneous surface (approximately in the center of the samples) of each sample was selected for IR measurements. The focused beam was about 200  $\mu\text{m}$  in size.

Raman spectra were obtained with a Renishaw RM1000 confocal micro-Raman spectrometer with a 20 mW, 632 nm He-Ne-laser excitation system and a thermo-electrically cooled CCD detector. The power of the laser beam on the sample was approximately 3 mW. Spectra were obtained in the range of 100–1200  $\text{cm}^{-1}$ , with approximately 30 sec total exposure time. The spectral resolution (apparatus function) was 4  $\text{cm}^{-1}$ . Areas of approximately  $400 \times 400 \mu\text{m}$  and  $600 \times 600 \mu\text{m}$  were selected for CL and BSE imaging. Raman spectra were taken from a volume equivalent to about  $3 \times 3 \times 3 \mu\text{m}$ , and CL spectra were obtained from areas of approximately  $40 \times 40 \mu\text{m}$ . Three CL spectra and three Raman spectra were acquired for different areas of each sample; because of the similarity of the spectra, it was not necessary to obtain more spectra per sample.

The thin sections were carbon-coated and examined with an Oxford Mono-CL system attached to a JEOL JSM 6400 scanning electron microscope (SEM). The operating conditions for all SEM-CL investigations were 15 kV accelerating voltage and 1.2 nA beam current. CL spectra were recorded (at room temperature) in the wavelength range of 200–800 nm, with 1 nm resolution from areas of  $60 \times 40 \mu\text{m}$ . The grating of the monochromator was 1200 lines/mm.

The energy-dispersive X-ray (EDX) analyses were carried out on the JEOL JSM-6400 scanning electron microscope equipped with a KEVEX system and performed as “standardless” analyses, with results normalized to a total of 100 wt%. The operation conditions were: 15 kV acceleration voltage, 1.5 nA sample current, and 40 sec counting time. The contents of eleven major element oxides ( $\text{SiO}_2$ ,  $\text{TiO}_2$ ,  $\text{Al}_2\text{O}_3$ ,  $\text{FeO}$ ,  $\text{MnO}$ ,  $\text{MgO}$ ,  $\text{CaO}$ ,  $\text{Na}_2\text{O}$ ,  $\text{K}_2\text{O}$ ,  $\text{Cr}_2\text{O}_3$ ,  $\text{P}_2\text{O}_5$ ) were determined.

## RESULTS

### Backscattered Electron and Cathodoluminescence Image Observations

#### *Aouelloul Impact Glass*

The backscattered electron (BSE) and cathodoluminescence (CL) images of the Aouelloul impact glass exhibits variation in the BSE brightness (Fig. 1a) and CL intensities (Fig. 1b). Table 1 gives the major element compositions of twenty points analyzed on the Aouelloul sample, and Fig. 2 shows the locations of the analyzed points (AOL-1 . . . 20) in the CL-bright and CL-dark areas of the glass. The CL-dark parts have relatively low  $\text{SiO}_2$  (81.7–87.5 wt%) and high  $\text{Al}_2\text{O}_3$  (6.9–9.6 wt%) contents, while the CL-bright areas have relatively high  $\text{SiO}_2$  (98.3–98.6 wt%) and low  $\text{Al}_2\text{O}_3$  (0.7–0.3 wt%) contents (Figs. 2a and 2b; Table 1). These CL-bright areas have elongated to rounded shapes with a variety of sizes (Figs. 1a and 1b).

The chemical data are in excellent agreement with Koeberl and Auer (1991) and Chaussidon and Koeberl (1995). These authors concluded that the low  $\text{SiO}_2$ /high

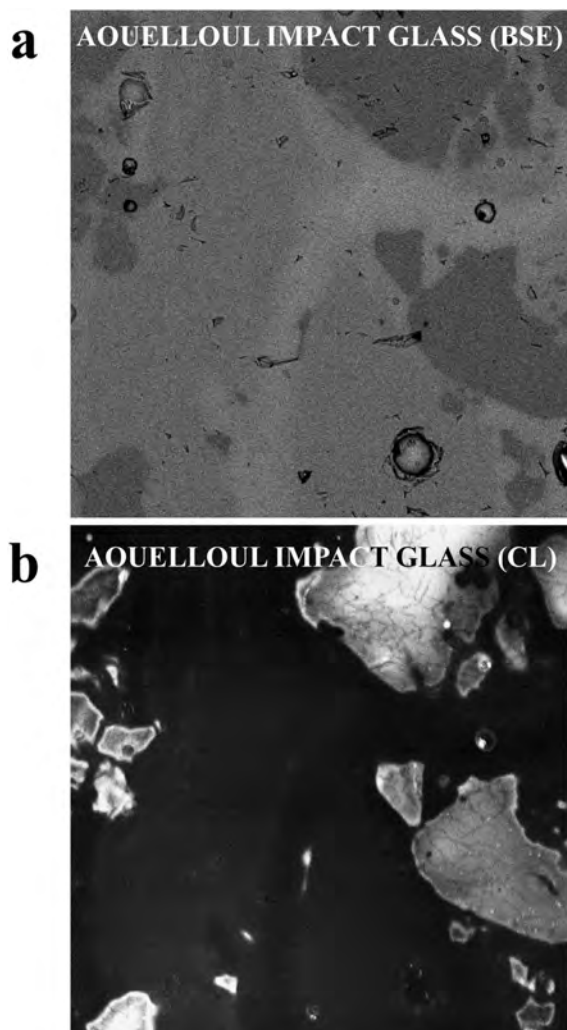


Fig. 1. Backscattered electron (BSE) image (a) and cathodoluminescence image (b) of Aouelloul impact glass show an inverse relationship between the brightness of the BSE signal and the corresponding cathodoluminescence intensity. The dark areas are related to the silica-rich composition, and bright regions are silica-poor areas in the BSE image. The images are  $\sim 400 \mu\text{m}$  wide.

$\text{Al}_2\text{O}_3$  parts of the impact glass might be derived from the Zli sandstone, which is one of the target rocks at the Aouelloul crater. Additionally, we observed partly digested apatite inclusions (e.g., spot AOL-16 in a CL-dark area).

#### *Muong Nong-Type Tektite*

The Muong-Nong-type tektite sample shows only minor variations in the brightness of the BSE images compared to those of the Aouelloul impact glass (Fig. 3a). Figure 4 shows the locations of the analyzed points (MNT-1 . . . 7) of the CL-bright and CL-dark areas of sample. In some areas, slightly darker bands or streaks are visible in the BSE image, which appear as CL-bright regions in the otherwise non-luminescent background of the CL image (Fig. 3). The data in Table 2 (and Fig. 4) indicate that the CL-dark parts are silica-poor areas ( $\text{SiO}_2$  of 78.7–82.7 wt%;  $\text{Al}_2\text{O}_3$  of 12.8–

Table 1. Major element composition of Aouelloul impact glass, showing variations between the CL-dark and CL-bright areas. The values are in wt%, and the numbers of the analyzed locations are indicated in the CL images of Fig. 2.

AOL-	1 (CL-dark)	2 (CL-bright)	3 (CL-bright)	4 (CL-bright)	5 (CL-dark)	6 (CL-dark)	7 (CL-dark)	8 (CL-dark)	9 (CL-dark)	10 (CL-dark)
SiO <sub>2</sub>	86.5	98.3	98.4	98.6	86.5	86.1	87.3	85.4	87.2	85.9
TiO <sub>2</sub>	0.38	0.22	0.16	0.14	0.45	0.31	0.22	0.55	0.43	0.49
Al <sub>2</sub> O <sub>3</sub>	7.78	0.66	0.55	0.37	7.40	7.90	7.46	7.91	7.19	7.59
FeO	2.00	0.08	0.18	0.17	1.81	1.90	2.16	2.25	2.06	1.56
MnO	0.14	0.18	0.13	0.13	0.25	0.03	0.18	0.20	0.08	0.04
MgO	0.89	0.07	0.05	0.02	0.39	1.59	0.15	0.57	0.61	1.08
CaO	0.38	0.13	0.09	0.06	0.46	0.19	0.41	0.52	0.37	0.48
Na <sub>2</sub> O	0.03	0.05	0.05	0.06	0.26	0.20	0.11	0.09	0.02	0.39
K <sub>2</sub> O	1.64	0.14	0.16	0.15	1.71	1.61	1.82	1.91	1.67	1.76
Cr <sub>2</sub> O <sub>3</sub>	0.15	0.09	0.19	0.23	0.15	0.05	0.14	0.16	0.16	0.09
P <sub>2</sub> O <sub>5</sub>	0.11	— <sup>a</sup>	—	—	0.54	0.07	—	0.38	0.10	0.54
Total	100.0	99.92	99.96	99.93	99.92	99.95	99.95	99.94	99.89	99.92
AOL-	11 (CL-dark)	12 (CL-bright)	13 (CL-dark)	14 (CL-dark)	15 (CL-dark)	16 (CL-dark)	17 (CL-dark)	18 (CL-dark)	19 (CL-dark)	20 (CL-dark)
SiO <sub>2</sub>	86.8	98.4	87.5	87.3	84.7	80.8	81.7	85.5	84.6	86.9
TiO <sub>2</sub>	0.39	0.09	0.54	0.32	0.60	0.52	1.08	0.75	0.27	0.52
Al <sub>2</sub> O <sub>3</sub>	7.89	0.74	7.22	7.10	8.39	6.85	9.60	7.99	9.04	6.90
FeO	1.92	0.18	1.43	2.27	2.20	3.25	2.83	2.01	2.11	2.34
MnO	0.16	0.09	0.27	0.12	0.22	0.12	0.30	0.19	0.05	0.25
MgO	0.30	0.07	0.50	0.43	1.32	0.50	1.14	0.59	1.52	0.44
CaO	0.39	0.11	0.44	0.29	0.38	0.39	0.51	0.43	0.34	0.40
Na <sub>2</sub> O	0.03	0.15	—	0.07	0.07	0.03	0.06	—	0.04	0.11
K <sub>2</sub> O	1.95	0.08	1.85	1.81	1.87	1.80	2.19	2.11	1.84	1.74
Cr <sub>2</sub> O <sub>3</sub>	0.11	0.05	0.23	0.16	0.22	0.19	0.37	0.19	0.05	0.18
P <sub>2</sub> O <sub>5</sub>	—	—	—	0.06	—	5.52	0.18	0.15	0.10	0.18
Total	99.94	99.96	99.98	99.93	99.97	99.97	99.96	99.91	99.96	99.96

<sup>a</sup>Below detection limit (0.03 wt%).

Table 2. Major element composition of CL-dark and CL-light areas in the Muong Nong-type tektite. The values are in wt% and the numbers of analyzed locations are indicated in the CL images of Fig. 4.

MNT-	1 (CL-dark)	2 (CL-bright)	3 (CL-bright)	4 (CL-dark)	5 (CL-dark)	6 (CL-dark)	7 (CL-dark)
SiO <sub>2</sub>	78.7	96.8	96.8	80.1	82.0	82.7	82.4
TiO <sub>2</sub>	0.55	0.19	0.26	0.67	0.41	0.47	0.40
Al <sub>2</sub> O <sub>3</sub>	12.8	1.17	1.09	12.0	10.2	9.02	10.0
FeO	3.72	0.63	0.48	2.86	2.29	3.29	3.12
MnO	0.14	0.20	0.18	0.19	0.07	0.46	0.12
MgO	0.67	0.03	0.14	0.65	0.69	0.17	0.50
CaO	0.92	0.09	0.11	0.92	1.11	0.95	0.89
Na <sub>2</sub> O	— <sup>a</sup>	0.08	0.26	0.39	0.90	0.58	0.43
K <sub>2</sub> O	2.16	0.39	0.45	2.08	2.14	2.01	1.87
Cr <sub>2</sub> O <sub>3</sub>	0.07	0.09	0.07	0.10	0.10	0.25	0.09
P <sub>2</sub> O <sub>5</sub>	0.23	0.31	0.10	—	0.07	0.04	0.13
Total	99.96	99.98	99.93	99.96	99.6	100.01	99.95

<sup>a</sup>Below detection limit (0.03 wt%).

9 wt%), and the (few) CL-bright areas have higher SiO<sub>2</sub> (96.8 wt%) and lower Al<sub>2</sub>O<sub>3</sub> (~1 wt%) contents, probably representing lechatelierite, which is common in Muong Nong-type tektites (Koeberl 1992). Thus, the CL-bright areas could be melted or partly digested remnants of quartz grains.

#### Libyan Desert Glass

Compared to the Aouelloul impact glass and Muong Nong-type tektite samples, this sample does not show any obvious variations in the BSE brightness (Figs. 5a and 5c) but exhibits a spectacularly varied appearance in the CL images (Figs. 5b and 5d). Table 3 reports the compositional data, and

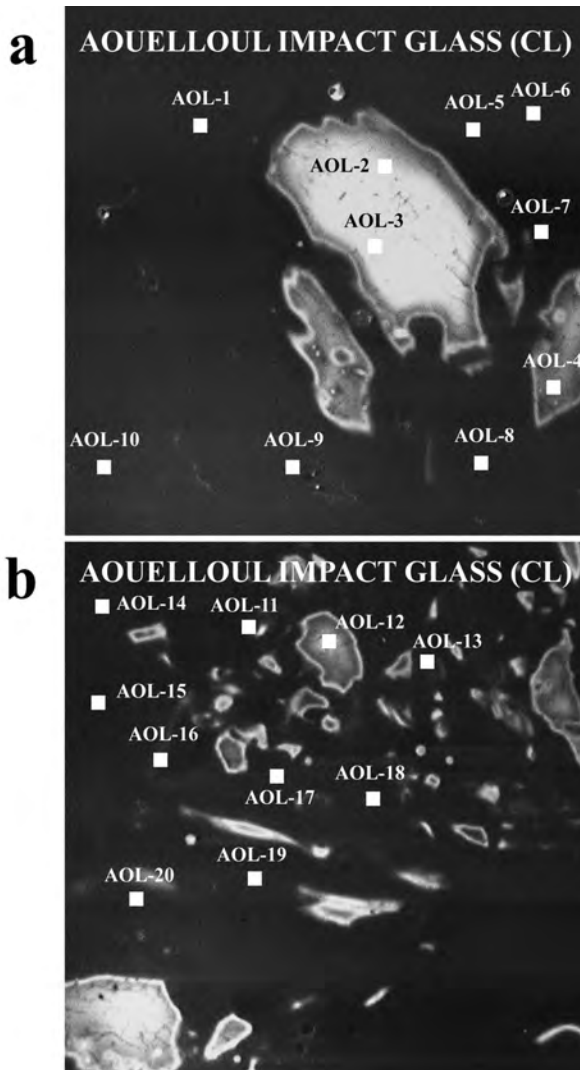


Fig. 2. Cathodoluminescence images of Auouelloul impact glass showing the locations of the analyzed points (numbers indicated in Table 1). The images are  $\sim 400 \times 400 \mu\text{m}$ .

Fig. 6 shows the locations of the analyzed spots. The CL images of the Libyan desert glass show predominantly CL-bright areas (Figs. 5b and 5d). As for the other studied glasses, the CL-dark parts are associated with relatively low  $\text{SiO}_2$  (92.8–97.8 wt%) and high  $\text{Al}_2\text{O}_3$  (0.6–2.3 wt%) contents, and the CL-bright areas have higher  $\text{SiO}_2$  (96.4–98.1 wt%) and lower  $\text{Al}_2\text{O}_3$  (0.4–1.7 wt%) abundances (Table 3). Our analyses agree with published data (e.g., Barrat et al. 1997). Figures 5b and 5d show that, in some cases, the CL-dark areas have zoned rims (or layers) with variations in the CL intensities. These areas have lower  $\text{SiO}_2$  and higher  $\text{Al}_2\text{O}_3$  contents compared to the CL-bright background (Figs. 6a and 6b) (Table 3). The high content of the  $\text{SiO}_2$  (as activator) in the CL-bright areas can generate more recombination centers for photon emission. The presence of trace elements (e.g., Fe or Ti) has quenching effects that are visible in the form of CL-dark zonations in the otherwise CL-bright background. Spot

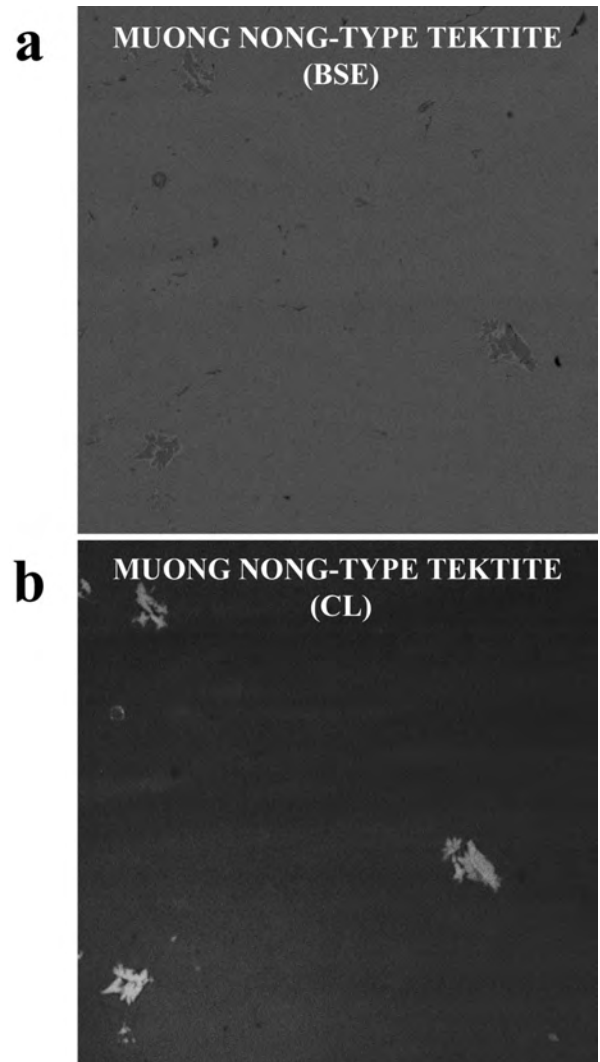


Fig. 3. Backscattered electron (BSE) image (a) and cathodoluminescence image (b) of Muong Nong-type tektite show an inverse relationship between the brightness of the BSE signal and the corresponding cathodoluminescence intensity. The CL-bright area is lechatelierite, which is a fused glass of quartz at a very high temperature ( $\sim 1700 \text{ }^\circ\text{C}$ ). The images are  $\sim 400 \times 400 \mu\text{m}$ .

LYD-5 (CL-bright) has relatively low  $\text{SiO}_2$  but high Ti, Mn, Cr, and Fe contents, which may indicate the presence of a dissolved accessory mineral or desert varnish from target sandstones.

### Infrared Spectra

The infrared (IR) spectrum of the Auouelloul impact glass contains a major peak at  $1106 \text{ cm}^{-1}$  and a relatively weak peak at  $769 \text{ cm}^{-1}$  (Fig. 7a). The Muong Nong-type tektite exhibits a major peak at  $1082 \text{ cm}^{-1}$  and a relatively weak band at  $747 \text{ cm}^{-1}$  (Fig. 7b), and the LDG spectrum has these features at  $1043 \text{ cm}^{-1}$  and  $740 \text{ cm}^{-1}$ , respectively (Fig. 7c). A common feature of the IR spectra of all samples is the appearance of major peaks between  $1043$  and  $1106 \text{ cm}^{-1}$  with minor peaks

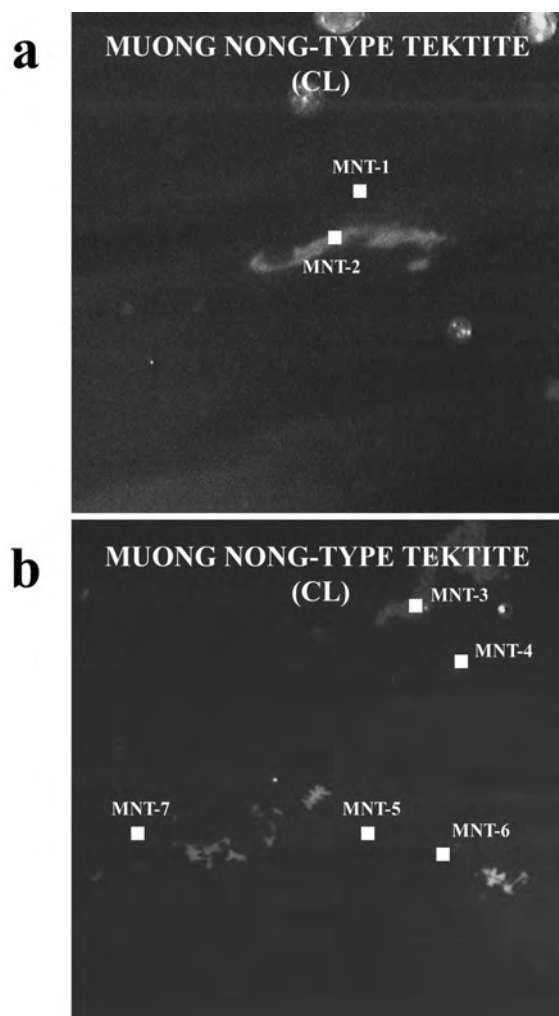


Fig. 4. Cathodoluminescence images of Muong Nong-type tektite exhibiting the locations of the analyzed points (the numbers are indicated in Table 2). The images are  $\sim 400 \mu\text{m}$  wide.

between  $745$  and  $769 \text{ cm}^{-1}$ . The major peaks have shoulders on both the left and the right flanks; this effect is most pronounced for the Auelloul glass.

Faulques et al. (2001) found a doublet at  $1106$ – $1230 \text{ cm}^{-1}$  and a single peak at  $783 \text{ cm}^{-1}$  in their Libyan desert glass sample, and they also reported systematic changes in the intensities of the IR spectra as a function of increasing  $\text{SiO}_2$  content.

### Raman Spectra

Common features in the Raman spectra of three impact glasses studied here are two broad bands at  $491$  and  $821 \text{ cm}^{-1}$  (Fig. 8). The broad band at  $821 \text{ cm}^{-1}$  is more pronounced in the Auelloul impact glass sample than in other samples. Additionally, a narrow band appears at  $676 \text{ cm}^{-1}$  in the Muong Nong-type tektite (Fig. 8).

In general, the Raman spectra of crystalline phases show

mainly narrow bands of stretching vibration (antisymmetric or symmetric) modes and a low level of background fluorescence. However, the high intensity of background in our samples (or the high level of background fluorescence) and the presence of broad bands (without any narrow bands) indicate a highly disordered state (low crystallinity).

### Cathodoluminescence Spectra

Figure 9 shows a comparison of typical CL spectra of the three different impact glasses, and also indicates the areas from which the spectra were taken. The CL spectrum of the Auelloul impact glass exhibits a doublet broad band at about  $330$ – $440 \text{ nm}$  (Fig. 9a), the Muong Nong-type tektite has a major broad band centered at  $440 \text{ nm}$  (Fig. 9b), and the Libyan desert glass spectrum exhibits a dominant broad band with a maximum at about  $390 \text{ nm}$  (Fig. 9c). A significant broad band at  $332$ – $444 \text{ nm}$  is common to the CL spectra of all three glasses. They do not contain narrow emission peaks that would indicate the presence of activator elements in the near-ultraviolet and visible light range.

We checked cathodoluminescence spectra of the embedding epoxy resin and of the glass slide used for mounting the samples and found that these materials do not produce, or contribute to, the broad bands observed.

## DISCUSSION

### Infrared Spectra

The major peaks at  $1106 \text{ cm}^{-1}$  (Auelloul impact glass),  $1082 \text{ cm}^{-1}$  (Muong Nong-type tektite), and  $1043 \text{ cm}^{-1}$  (Libyan desert glass) indicate the presence of the antisymmetric stretching vibration of the  $\text{SiO}_4$  tetrahedra. In all samples, the shoulder peaks, as intermediate frequency modes between  $745$  and  $769 \text{ cm}^{-1}$ , are associated with the Si-O-Si angle deformation. Compared to the analogous modes of quartz and coesite (Williams et al. 1993), the frequency shift of these bands indicates the presence of amorphous quartz.

### Raman Spectra

McMillan (1984), from his structural studies of silicate glasses and melts, suggested that the bands in the  $1200$ – $800 \text{ cm}^{-1}$  region can be assigned to silicon-oxygen stretching vibrations of tetrahedral silicate units. The weak high-frequency bands of silica glass have been assigned to antisymmetric stretching vibrations of silicate tetrahedra within a fully polymerized tetrahedral silicate network. White and Minser (1984), in their Raman studies of natural glasses (e.g., desert glass, tektites and obsidians of various composition, and some lunar glasses), noted that the wave number of the  $400$ – $600 \text{ cm}^{-1}$  band varies with the degree of

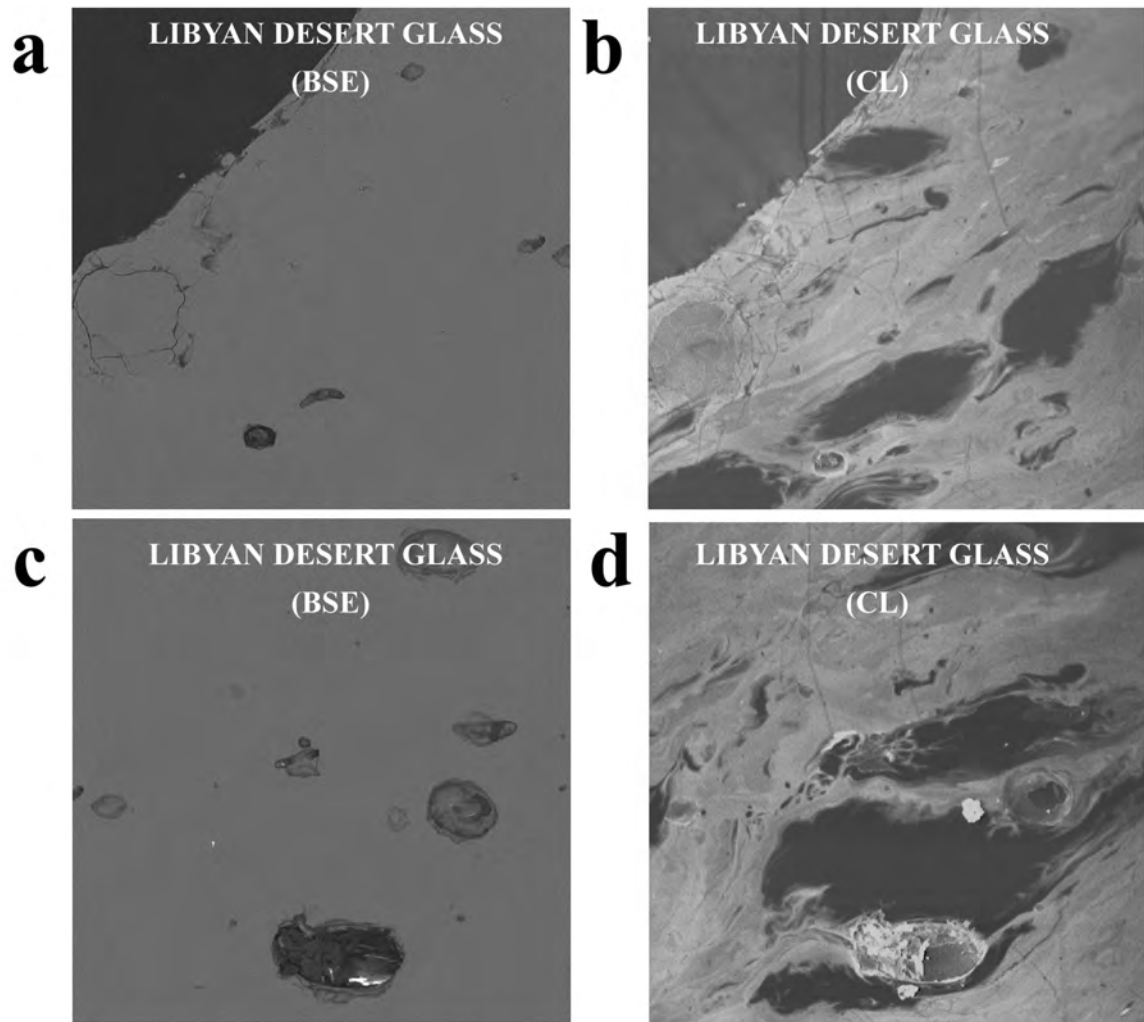


Fig. 5. Backscattered electron (BSE) (a, c) and cathodoluminescence (CL) (b, d) images of Libyan desert glass do not exhibit an inverse relationship between the brightness of the BSE signal and the corresponding cathodoluminescence intensity. The CL-dark (with a relatively low  $\text{SiO}_2$  content) areas show rims as zonations (or layers) with variations in the CL intensities in an otherwise CL-bright (silica-rich) background. The images are  $\sim 600 \times 600 \mu\text{m}$ .

polymerization of the network and with Si-O-Si (and Si-O-Al) bridging bond angles.

Raman properties of quartz amorphization by shock pressure have been reported from different impact environments, including samples from shock recovery experiments of quartz (e.g., Hemley et al. 1986; McMillan et al. 1992; Williams et al. 1993; Serghiou et al. 1995; Champagnon et al. 1996; Okuno et al. 1999; Schmidt and Ziemann 2000), from impact structures (Vredefort impact structure: Halvorson and McHone 1992; Chicxulub impactites: Ostroumov et al. 2002), and from desert glasses and tektites (e.g., Faulques et al. 2001). It was suggested that peak shifts and the occurrence of a new band in quartz might be associated with formation of high density  $\text{SiO}_2$ . The presence of cristobalite inclusions in Libyan desert glass (LDG) was confirmed by Raman spectroscopy by McHone et al. (2000), who found three strong Raman peaks at 114, 231, and  $418 \text{ cm}^{-1}$ .

The broad Raman bands at  $491$  and  $821 \text{ cm}^{-1}$ , which are present in all of our samples, are probably indicating remnants of diaplectic glass, as already noted by McMillan et al. (1992). These authors also suggested that the formation mechanism of diaplectic glass could be related to a metastable melting event or spinodal lattice collapse on attainment of a mechanical stability limit of crystalline quartz. The narrow peak at  $676 \text{ cm}^{-1}$  in the Raman spectrum of the Muong Nong-type tektite indicates a Si-O stretching vibrational mode (McMillan 1984).

### Cathodoluminescence Investigations

#### *CL-Bright and CL-Dark Areas in Cathodoluminescence (CL) Images*

In general, the BSE contrast is related to the average atomic number ( $Z$ ) of components (Kempe et al. 2000). In

Table 3. Major element composition of CL-dark and CL-bright areas in Libyan desert glass. The values are in wt% and the numbers of analyzed locations are indicated in the CL images of Fig. 6.

LYD-	1 (CL-bright)	2 (CL-bright)	3 (CL-bright)	4 (CL-dark)	5 (CL-bright)	6 (CL-dark)	7 (CL-dark)	8 (CL-bright)	9 (CL-bright)
SiO <sub>2</sub>	96.7	97.2	98.1	96.8	60.4	96.9	97.8	97.3	96.7
TiO <sub>2</sub>	0.22	0.18	0.38	0.15	7.17	0.22	0.27	0.19	0.06
Al <sub>2</sub> O <sub>3</sub>	1.37	0.92	0.49	0.83	0.77	0.07	0.61	1.25	1.70
FeO	0.04	0.55	0.26	0.09	14.1	0.26	0.16	0.09	0.09
MnO	0.14	– <sup>a</sup>	0.33	0.48	9.89	0.09	0.14	0.34	–
MgO	0.30	0.17	–	0.45	0.28	0.03	0.12	0.09	0.38
CaO	0.18	0.14	0.13	0.09	0.70	1.88	0.25	0.08	0.15
Na <sub>2</sub> O	0.43	0.30	0.04	0.40	–	0.03	0.11	0.11	0.26
K <sub>2</sub> O	0.26	0.11	0.05	0.22	0.75	–	0.14	0.12	0.12
Cr <sub>2</sub> O <sub>3</sub>	0.19	0.07	0.14	0.35	5.15	0.25	0.22	0.28	0.22
P <sub>2</sub> O <sub>5</sub>	0.13	0.33	–	0.11	0.71	0.26	0.15	0.08	0.23
Total	99.96	99.97	99.92	99.97	99.92	99.99	99.97	99.93	99.91
LYD-	10 (CL-bright)	11 (CL-dark)	12 (CL-dark)	13 (CL-dark)	14 (CL-bright)	15 (CL-bright)			
SiO <sub>2</sub>	97.5	92.8	95.8	95.7	97.7	96.4			
TiO <sub>2</sub>	0.13	0.85	0.30	0.35	0.28	0.23			
Al <sub>2</sub> O <sub>3</sub>	0.94	1.96	1.97	2.39	0.75	1.56			
FeO	–	1.06	0.22	–	0.37	0.14			
MnO	0.44	0.92	0.13	0.09	0.08	0.13			
MgO	0.51	0.58	0.42	0.29	0.42	0.34			
CaO	0.04	0.17	0.23	0.10	0.05	0.30			
Na <sub>2</sub> O	0.20	0.25	0.15	0.30	0.09	0.31			
K <sub>2</sub> O	–	0.27	0.21	0.38	0.07	0.11			
Cr <sub>2</sub> O <sub>3</sub>	0.23	1.04	0.23	0.10	0.04	0.16			
P <sub>2</sub> O <sub>5</sub>	0.02	0.07	0.24	0.21	0.09	0.27			
Total	100.01	99.70	99.90	99.91	99.94	99.95			

<sup>a</sup>Below detection limit (0.03 wt%).

general, the higher Z elements produce higher BSE yield (e.g., bright BSE parts of the image). In our samples, the BSE images of the tektite were almost featureless, while the Libyan desert glass and, especially, the Auouelloul glass showed more variation in contrast and brightness.

The CL images of our samples show more variety than the BSE images. In all three cases, brightness and contrast variations are inversely correlated between the BSE and the CL images, and features that appear in the BSE image can usually also be discerned in the CL image. In fact, the CL images show more pronounced contrast and brightness variations than the BSE images. The CL images seem to preserve target rock textures much better than any other electron image, even though the samples appear to be totally glassy. The Auouelloul sample clearly shows a granular texture (Figs. 1 and 2), which is probably preserving the texture of the original sandstone. The CL images of the Libyan desert glass (Figs. 5 and 6) are most spectacular and show a distorted original texture, probably indicating high temperature glass flow; no such features are apparent in optical or BSE images. The inverse relationship between BSE and CL brightness is caused by high concentrations of Al, Li, and Na (Ramseyer et al. 1988; Ramseyer and Mullis 1990; Perny et al. 1992; Demars et al. 1996).

#### Broad Bands in the CL Spectrum

Broad bands in the CL spectrum indicate that excited and ground states of the electronic radiative transitions are strongly coupled with the vibrating lattice (Remond et al. 2000). According to Stevens Kalceff et al. (2000, and references therein), the normal defect-free configuration of (low pressure) silicon dioxide polymorphs can be represented as (=Si-O-Si=), indicating that each silicon atom is surrounded by four tetrahedrally configured oxygen atoms, and the adjacent silicon atoms are bridge bonded through a single oxygen atom. The silicon dioxide structure may be modified by the presence of defects (e.g., impurities, vacancies, etc.). The detected luminescence bands of the crystalline and amorphous modifications of SiO<sub>2</sub> are attributed to three optical active luminescence centers: two-fold coordinated silicon (=Si:), non-bridging oxygen hole center, and the self-trapped exciton (STE) (Fitting et al. 2001).

Thus, the two broad bands observed at 332 (3.73 eV) and around 440 nm (2.79 eV) in the cathodoluminescence spectra of Auouelloul impact glass and Muong Nong-type tektite are related to the presence of such defect centers. The broad band at 332 nm (3.73 eV) can be attributed to the dominant defects that occur in the short-range order involving the slightly distorted SiO<sub>4</sub> tetrahedra. These defects are common to both

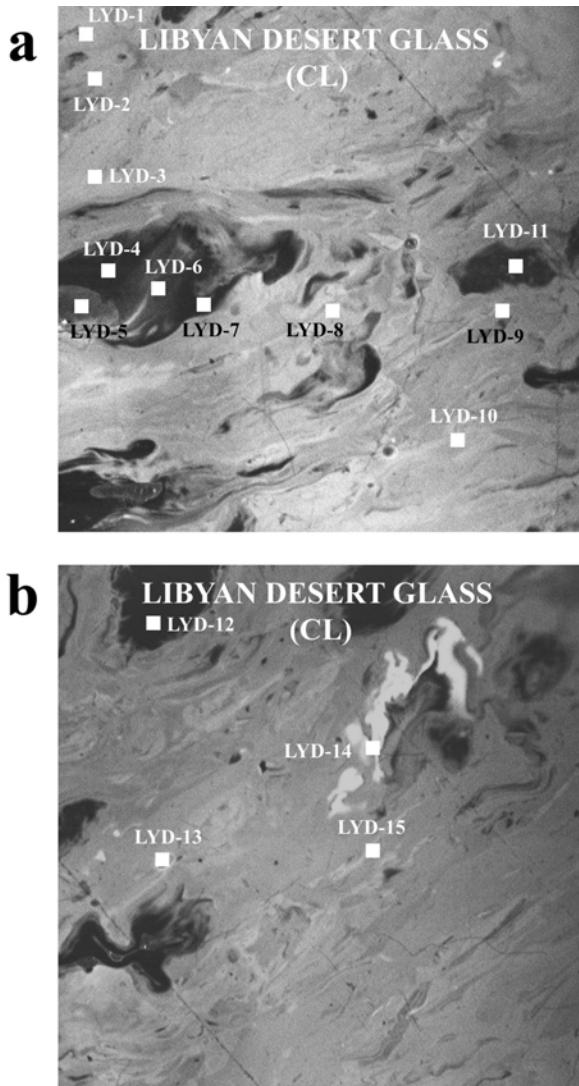


Fig. 6. Cathodoluminescence images of Libyan desert glass exhibiting the locations of the analyzed points (the numbers are indicated in Table 3). The images refer to  $\sim 600 \times 600 \mu\text{m}$  areas.

the crystalline and amorphous  $\text{SiO}_2$  structures (Fitting et al. 2001). The band at 444 nm (2.79 eV) is probably associated with the radiative relaxation of the STE in quartz, which is strongly polarized along the c-axis (Kalceff et al. 2000).

### SUMMARY AND CONCLUSIONS

A comparative spectroscopic investigation, involving infrared reflectance, Raman, and CL spectrometry, as well as BSE and CL images, was performed on a variety of impact glass samples. These included Auelloul impact glass, a Muong Nong-type tektite, and Libyan desert glass. These glasses were selected because they represent the range from locally produced impact glass (in a small event) to impact glass from a medium-magnitude event (Libyan desert glass) to a glass that experienced a high-energy

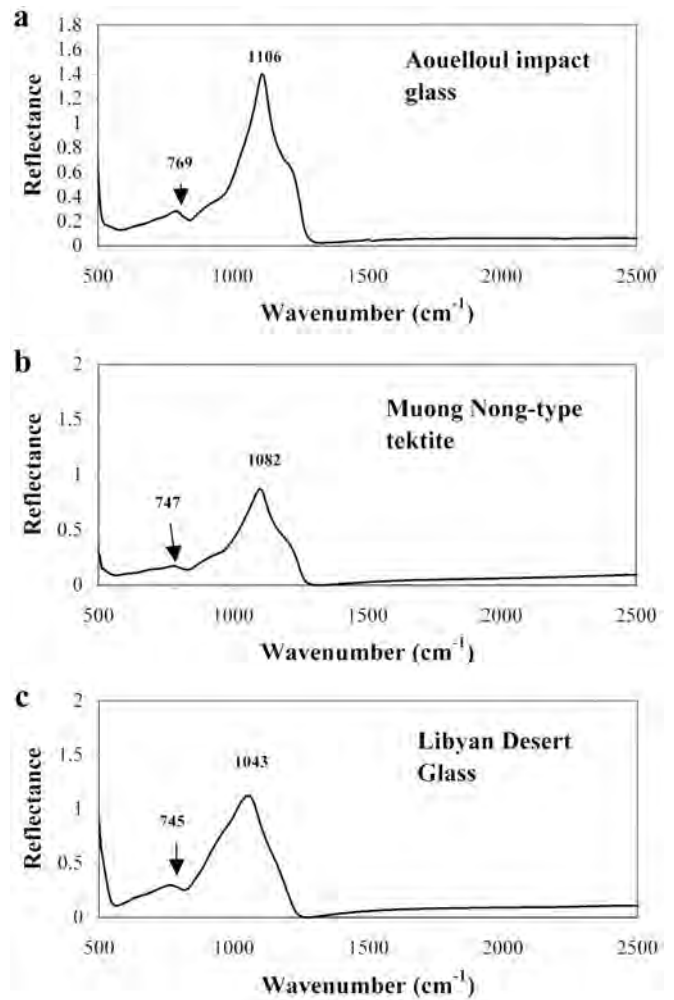


Fig. 7. Infrared (IR) reflectance spectra of Auelloul impact glass (a), Muong Nong-type tektite (b), and Libyan desert glass (c) generally show a significant peak at 1043–1106  $\text{cm}^{-1}$ , with smaller peaks at 745–769  $\text{cm}^{-1}$ .

event (indochinite). The results can be summarized as follows:

- The BSE images of the tektite and the Libyan desert glass are relatively featureless; only the Auelloul glass shows some contrast and brightness variations.
- The CL images of the tektite show only a few areas with brightness variations, while the Auelloul glass and the Libyan desert glass CL images show significant variations in contrast and brightness.
- There is an inverse relationship between BSE brightness and CL intensities, which is most pronounced for the Auelloul glass and less so for the tektite and the Libyan desert glass.
- Compositional analyses show that the CL-bright areas have higher  $\text{SiO}_2$  contents (and lower contents of other elements) than the CL-dark areas.
- The IR reflectance spectra of all samples are similar and negligible intrasample variations were observed. A broad

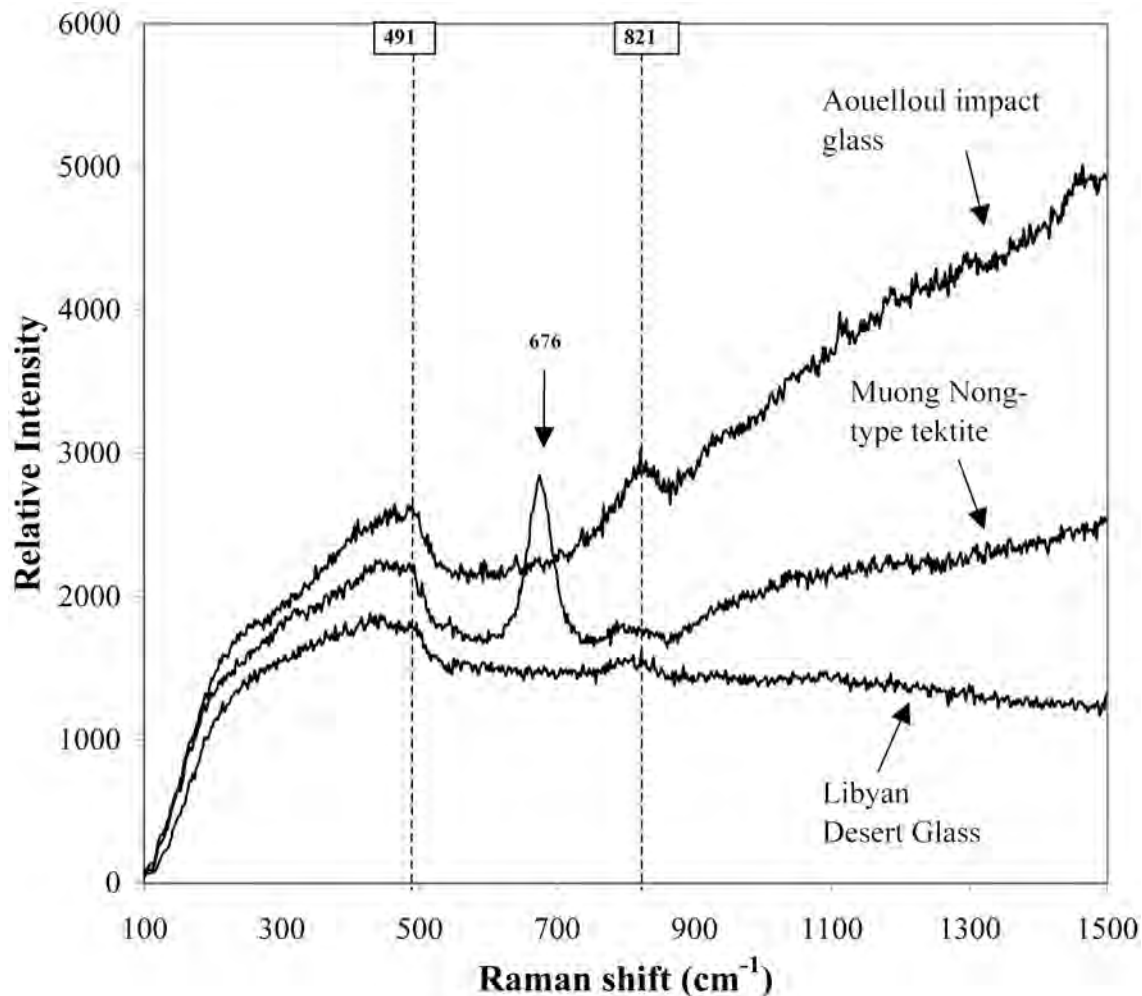


Fig. 8. Raman spectra of Auelloul impact glass (a), Muong Nong-type tektite (b), and Libyan desert glass (c) generally exhibit two broad bands at 491 and 821  $\text{cm}^{-1}$  and relatively high background fluorescence, which indicate a high degree of amorphization. These broad bands might be due to diaplectic glass. The numbers denote peak positions in  $\text{cm}^{-1}$ .

peak appears in the IR spectrum of each sample, between about 1040 and 1100  $\text{cm}^{-1}$ , which is correlated to the antisymmetric stretching vibrations of the  $\text{SiO}_4$  tetrahedra; minor peaks at about 745–770  $\text{cm}^{-1}$  are probably related to deformations in the Si-O-Si bond angle.

- Raman spectra of all glasses have a high fluorescence background and contain broad bands at 491 and 821  $\text{cm}^{-1}$ ; these could be associated with diaplectic glass. A narrow peak at 676  $\text{cm}^{-1}$  in the tektite, a Raman spectrum is probably related to Si-O stretching vibrations.
  - The CL spectra also show little intrasample variation; in the case of the tektite and the Libyan desert glass, only one broad band, centered at 440 and 390 nm, respectively, is present in the CL spectrum (range 200 to 800 nm), while the Auelloul glass sample shows a broad doublet with maxima at 332 and 444 nm.
- From these observations, we conclude the following:
- The tektite sample is the most homogeneous of the three

varieties of impact glasses in our study. This was expected, although, it was hoped that the Muong Nong-type tektite might show remnants of layering in the CL image (the contrast in atomic number is not pronounced enough to expect much of an effect in the BSE image).

- The Libyan desert glass shows little brightness variation in the BSE image, but the CL images of this glass are extremely rich in detail. In the case of the Auelloul impact glass, both BSE and CL images show some texture, but the effect is most pronounced in the CL image.
- In the case of the Auelloul glass, the CL-light and CL-dark areas are well-separated and confined and give the impression of a granular structure, probably preserving the texture of the source sandstone. On the other hand, the Libyan desert glass CL images, which reveal details that cannot be seen with any other microscopic method, indicate the presence of (high temperature) flow textures.
- Thus, it appears as if the maximum temperature (and

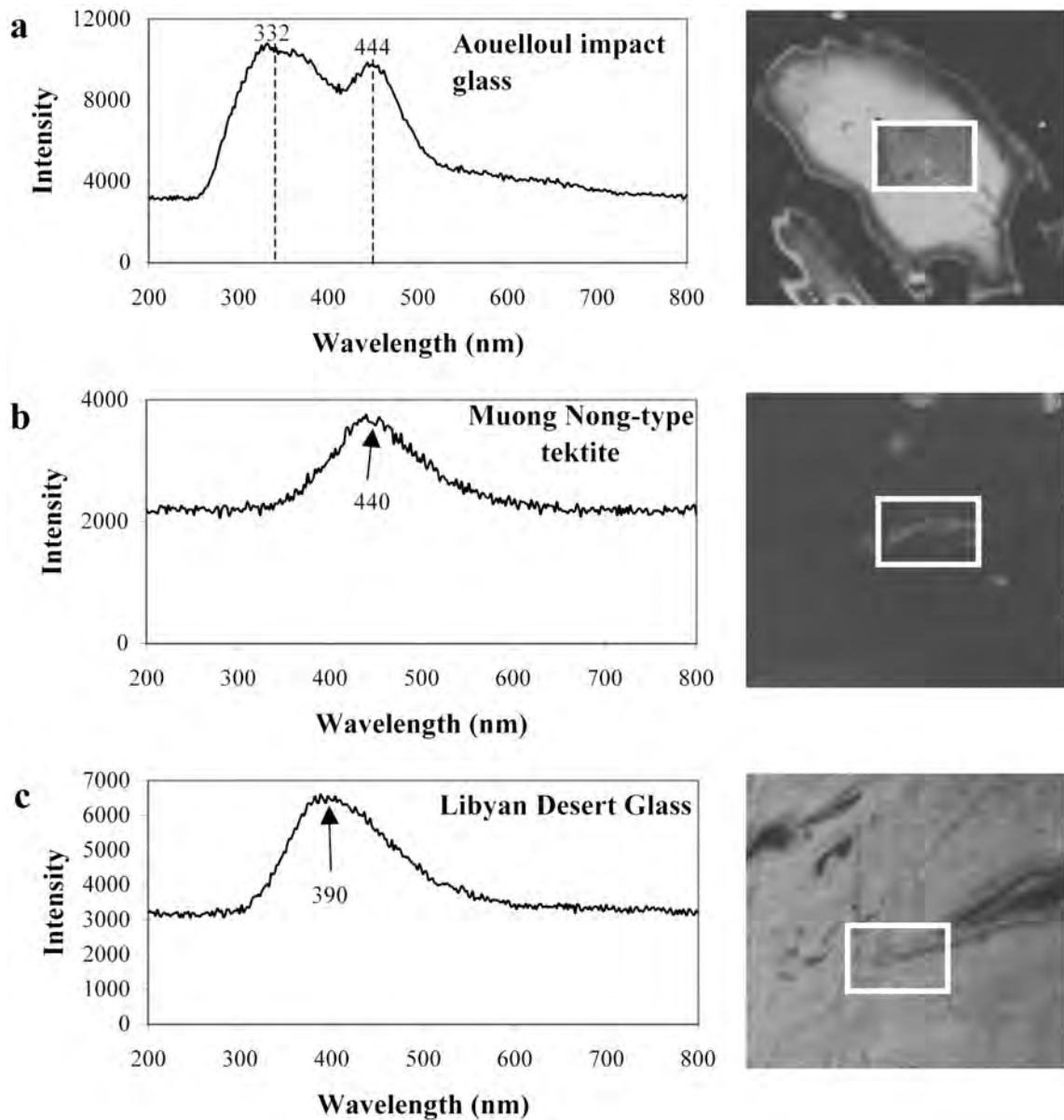


Fig. 9. Cathodoluminescence (CL) spectra of Auelloul impact glass (a), Muong Nong-type tektite (b), and Libyan desert glass (c) and CL images of the selected area (the white-rimmed squares refer to  $60 \times 40 \mu\text{m}$  areas) in the right part of this figure. The broad bands in all samples might be due to defect centers in slightly distorted  $\text{SiO}_4$  tetrahedra. The numbers denote peak positions in nm.

degree of homogenization) experienced by the three glass types increased from the Auelloul glass (textural features preserved in BSE and CL images: lowest temperature) to the Libyan desert glass (flow textures only in CL images: medium temperature), to the Muong Nong-type tektite (almost featureless in BSE and CL images: highest temperature). This coincides with the magnitude of the three glass-forming events as deduced from geological criteria and indicates that CL information can be used to obtain information about the peak formation temperature of impact glasses.

- The Raman spectra of all samples have peaks that

indicate the presence of remnants of shock amorphization, e.g., diaplectic quartz glass, which may have formed early in the shock melting of the glass; later, the high temperature led to almost complete annealing (temperature amorphization).

Thus, we conclude that the combination of BSE and CL imaging and IR, CL, and Raman spectroscopy is a powerful tool that can be used to characterize the structure and temperature history of these impact glass samples. Our results also give new insights into the structural changes that occur in these specimens during shock metamorphism and the pressures associated with these changes.

*Acknowledgments*—We thank Gero Kurat (Natural History Museum, Vienna, Austria) for access to the SEM-CL facility at the Natural History Museum, Vienna, Austria. Laboratory work was supported by the Austrian Science Foundation (grant Y58-GEO to C. Koeberl). A. Gucsik also thanks Monica M. Grady for funding from the F. A. Paneth Meteorite Trust of the Royal Astronomical Society Vacation Internship Programme at the University of Cambridge, Department of Earth Sciences, UK. We appreciate critical and constructive reviews by A. Basu and V. Hamilton.

*Editorial Handling*—Dr. Carlé Pieters

## REFERENCES

- Barnes V. E. and Underwood J. R. 1976. New investigations of the strewn field of the Libyan desert glass and its petrography. *Earth and Planetary Science Letters* 30:117–122.
- Barrat J. A., Jahn B. M., Amosse J., Rocchia R., Keller F., Poupeau G. R., and Diemer E. 1997. Geochemistry and origin of Libyan desert glasses. *Geochimica et Cosmochimica Acta* 61:1953–1959.
- Beran A. and Koeberl C. 1997. Water in tektites and impact glasses by FTIR spectrometry. *Meteoritics & Planetary Science* 32:211–216.
- Bigazzi G. and De Michele V. 1996. New fission-track age determination on impact glasses. *Meteoritics & Planetary Science* 31:234–236.
- Boggs S., Krinsley D. H., Goles G. G., Seyedolali A., and Dypvik H. 2001. Identification of shocked quartz by scanning cathodoluminescence imaging. *Meteoritics & Planetary Science* 36:783–793.
- Champagnon B., Panczer G., Chemarin C., and Humbert-Labeaumaz B. 1996. Raman study of quartz amorphization by shock pressure. *Journal of Non-Crystalline Solids* 196:221–226.
- Chaussidon M. and Koeberl C. 1995. Boron content and isotopic composition of tektites and impact glasses: Constraints on source regions. *Geochimica et Cosmochimica Acta* 59:613–624.
- Cipriani C., Corazza M., Giuli G., Cecchi V. N., Pratesi G., Rossi P., and Vittone E. 2000. Ion beam study of a possible extraterrestrial body signature in Libyan desert glass. *Nuclear Instruments and Methods in Physical Research B* 170:187–192.
- Deloule E., Chaussidon M., Glass B. P., and Koeberl C. 2001. U-Pb isotopic study of relict zircon inclusions recovered from Muong Nong-type tektite. *Geochimica et Cosmochimica Acta* 65:1833–1838.
- Demars C., Pagel M., Deloule E., and Blanc P. 1996. Cathodoluminescence of quartz from sandstones: Interpretation of the UV range by determination of trace element distributions and fluid inclusion P-T-X properties in authigenic quartz. *American Mineralogist* 81:891–901.
- Diemer E. 1997. Libyan desert glass: An impactite. State of the art in July 1996. In *Silica '96*, edited by de Michele V. Milan: Pyramids. pp. 29–36.
- El Goresy A. 1965. Baddeleyite and its significance in impact glasses. *Journal of Geophysical Research* 70:3453–3456.
- El Goresy A., Fechtig H., and Ottemann T. 1968. The opaque minerals in impactite glasses. In *Shock metamorphism of natural materials*, edited by French B. M. and Short N. M. Baltimore: Mono Book Co. pp. 531–553.
- Faulques E., Fritsch E., and Ostroumov M. 2001. Spectroscopy of natural silica-rich glasses. *Journal of Mineralogical and Petrological Sciences* 96:120–128.
- Fitting H. J., Barfels T., Trukhin A. N., and Schmidt B. 2001. Cathodoluminescence of crystalline and amorphous SiO<sub>2</sub> and GeO<sub>2</sub>. *Journal of Non-Crystalline Solids* 279:51–59.
- Fudali R. F. 1981. The major element chemistry of Libyan desert glass and the mineralogy of its precursor. *Meteoritics* 16:247–259.
- French B. M. 1998. *Traces of catastrophe: A handbook of shock-metamorphic effects in terrestrial meteorite impact structures*. LPI Contribution No. 954. Houston: Lunar and Planetary Institute. 120 p.
- Fudali R. F. and Cressy P. J. 1976. Investigation of a new stony meteorite from Mauritania with some additional data on its find site: Aouelloul crater. *Earth and Planetary Science Letters* 30:262–268.
- Glass B. P. 1972. Crystalline inclusions in a Muong Nong-type indochinite. *Earth and Planetary Science Letters* 16:23–26.
- Glass B. P. 1990. Tektites and microtektites: Key facts and inferences. *Tectonophysics* 171:393–404.
- Gucsik A., Koeberl C., Brandstätter F., Libowitzky E., and Reimold W. U. 2003. Scanning electron microscopy, cathodoluminescence, and Raman spectroscopy of experimentally shock-metamorphosed quartzite. *Meteoritics & Planetary Science* 38:1187–1197.
- Halvorson K. and McHone J. F. 1992. Vredfort coesite confirmed with Raman spectroscopy (abstract). 23rd Lunar and Planetary Science Conference. pp. 477–478.
- Hayward C. L. 1998. Cathodoluminescence of ore and gangue minerals and its application in the minerals industry. In *Modern approaches to ore and environmental mineralogy*, edited by Cabri L. J. and D. J. Vaughan. Ottawa: Mineralogical Association of Canada. pp. 269–325.
- Hemley J. R., Mao K. H., Bell M. P., and Mysen O. B. 1986. Raman spectroscopy of SiO<sub>2</sub> glass at high pressure. *Physical Review Letters* 57:747–750.
- Horn P., Müller-Sohnius D., Schaaf P., Kleinmann B., and Storzer D. 1997. Potassium-argon and fission-track dating of Libyan desert glass, and strontium and neodymium isotope constraints on its source rocks. In *Silica '96*, edited by de Michele V. Milan: Pyramids. pp. 59–73.
- Kempe U., Gruner T., Nasdala L., and Wolf D. 2000. Relevance of cathodoluminescence for the interpretation of U-Pb zircon ages, with an example of an application to a study of zircons from the Saxonian granulite complex, Germany. In *Cathodoluminescence in geosciences*, edited by Pagel M., Barbin V., Blanc P., and Ohnenstetter D. Berlin: Springer. pp. 415–455.
- Koeberl C. 1986. Geochemistry of tektites and impact glasses. *Annual Review of Earth and Planetary Sciences* 14:323–350.
- Koeberl C. 1992. Geochemistry and origin of Muong Nong-type tektites. *Geochimica et Cosmochimica Acta* 56:1033–1064.
- Koeberl C. 1994. African meteorite impact craters: Characteristics and geological importance. *Journal of African Earth Sciences* 18: 263–295.
- Koeberl C. and Auer P. 1991. Geochemistry of impact glass from the Aouelloul crater, Mauritania (abstract). 22nd Lunar and Planetary Science Conference. pp. 731–732.
- Koeberl C., Reimold W. U., and Shirey S. B. 1998. The Aouelloul crater, Mauritania: On the problem of confirming the impact origin of a small crater. *Meteoritics & Planetary Science* 33:513–517.
- Marshall D. J. 1988. *Cathodoluminescence of geological materials*. Boston: Unwin Hyman. 146 p.
- Mashimo T., Nishii K., Soma T., and Sawaoka A. 1980. Some physical properties of amorphous SiO<sub>2</sub> synthesized by shock compression of  $\alpha$ -quartz. *Physics and Chemistry of Minerals* 5: 367–377.

- McHone J. F., Killgore M., and Kudryavtsev A. 2000. Cristobalite inclusions in Libyan desert glass: Confirmation using Raman spectroscopy (abstract #1877). 31st Lunar and Planetary Science Conference. CD-ROM.
- McMillan P. F. 1984. Structural studies of silicate glasses and melts: Applications and limitations of Raman spectroscopy. *American Mineralogist* 69:622–644.
- McMillan P. F. and Rimmelle L. F., Jr. 1986. Hydroxyl sites in SiO<sub>2</sub> glass: A note on infrared and Raman spectra. *American Mineralogist* 71:772–778.
- McMillan P. F., Wolf G. H., and Lambert P. 1992. A Raman spectroscopic study of shocked single crystalline quartz. *Physics and Chemistry of Minerals* 19:71–79.
- McMillan P. F., Poe T. B., Gillet Ph., and Reynard B. 1994. A study of SiO<sub>2</sub> glass and supercooled liquid to 1950 K via high temperature Raman spectroscopy. *Geochimica et Cosmochimica Acta* 58:3653–3664.
- McPherson D., Pye D. L., and Frechette D. V. 1984. Microstructure of natural glasses. *Journal of Non-Crystalline Solids* 67:61–79.
- Murali A. V., Zolensky M. E., Underwood J. R., Jr., and Giegengack R. F. 1997. Chondritic debris in Libyan desert glass. In *Silica '96*, edited by de Michele V. Milan: Pyramids. pp. 133–142.
- Okuno M., Reynard B., Shimada Y., Syono Y., and Willaime C. 1999. A Raman spectroscopic study of shock-wave densification of vitreous silica. *Physics and Chemistry of Minerals* 26:304–311.
- Ostroumov M., Faulques E., and Lounejeva E. 2002. Raman spectroscopy of natural silica in Chicxulub impactite, Mexico. *Comptes Rendus Geoscience* 334:21–26.
- Piazenza B. 1997. Evidence of granular structure of Libyan desert silica glass by SEM cathodoluminescence. In *Silica '96*, edited by de Michele V. Milan: Pyramids. pp. 85–90.
- Perny B., Eberhardt P., Ramseyer K., Mullis J., and Pankrath R. 1992. Microdistribution of Al, Li, and Na in  $\alpha$ -quartz: Possible causes and correlation with short-lived cathodoluminescence. *American Mineralogist* 77:534–544.
- Pratesi G., Viti C., Cipriani C., and Mellini M. 2002. Silicate-silicate liquid immiscibility and graphite ribbons in Libyan desert glass. *Geochimica et Cosmochimica Acta* 66:903–911.
- Ramseyer K. and Mullis J. 1990. Factors influencing short-lived blue cathodoluminescence of  $\alpha$ -quartz. *American Mineralogist* 75:791–800.
- Ramseyer K., Baumann J., Matter A., and Mullis J. 1988. Cathodoluminescence colors of  $\alpha$ -quartz. *Mineralogical Magazine* 52:669–677.
- Remond G., Phillips M. R., and Roques-Carnes C. 2000. Importance of instrumental and experimental factors on the interpretation of cathodoluminescence data from wide gap materials. In *Cathodoluminescence in geosciences*, edited by Pagel M., Barbin V., Blanc P., and Ohnenstetter D. Berlin: Springer. pp. 59–126.
- Roberts S. and Beattie I. 1995. Micro-Raman spectroscopy in the Earth sciences. In *Microprobe techniques in the Earth sciences*, edited by Potts P. J., Bowles J. F. W., Reed S. J. B., and Cave M. R. London: Chapman and Hall. pp. 387–408.
- Rocchia R., Robin E., Fröhlich F., Amosse J., Barrat J. A., Meon H., Froget L., and Diemer E. 1997. The impact origin of Libyan desert glass. In *Silica '96*, edited by de Michele V. Milan: Pyramids. pp. 143–149.
- Schmidt C. and Ziemann A. M. 2000. In situ Raman spectroscopy of quartz: A pressure sensor for hydrothermal diamond-anvil cell experiments at elevated temperatures. *American Mineralogist* 85:1725–1734.
- Serghiou G., Zerr A., Chudinovskikh L., and Boehler R. 1995. The coesite-stishovite transition in a laser-heated diamond cell. *Geophysical Research Letters* 22:441–444.
- Stevens Kalceff M. A., Phillips M. R., Moon A. R., and Kalceff W. 2000. Cathodoluminescence microcharacterisation of silicon dioxide polymorphs. In *Cathodoluminescence in geosciences*, edited by Pagel M., Barbin V., Blanc P., and Ohnenstetter D. Berlin: Springer. pp. 193–224.
- Storzer D. and Koeberl C. 1991. Uranium and zirconium enrichments in Libyan desert glass: Zircon, baddeleyite, and high temperature history of the glass (abstract). 22nd Lunar and Planetary Science Conference. pp. 1345–1346.
- Storzer D. and Wagner G. A. 1977. Fission track dating of meteorite impacts (abstract). *Meteoritics* 12:368.
- White B. W. and Minser G. D. 1984. Raman spectra and structure of natural glasses. *Journal of Non-Crystalline Solids* 67:45–59.
- Williams Q., Hemley J. R., Kruger B. M., and Jeanloz R. 1993. High pressure infrared spectra of  $\alpha$ -quartz, coesite, stishovite, and silica glass. *Journal of Geophysical Research* 98:22157–22170.
- Zhang M. and Salje E. K. H. 2001. Infrared spectroscopic analysis of zircon: Radiation damage and the metamict state. *Journal of Physics: Condensed Matter* 13:3057–3071.
- Zhang M., Salje E. K. H., and Ewing R. C. 2002. Infrared spectra of Si-O overtones, hydrous species and U ions in metamict zircon: Radiation damage and recrystallization. *Journal of Physics: Condensed Matter* 14:3333–3352.
-